

On capillary-gravity waves generated by a slow moving object

A. D. Chepelianskii^(a,b), F. Chevy^(c) and E. Raphaël^(a)

^(a) *Laboratoire Physico-Chimie Théorique, UMR CNRS Gulliver 7083, ESPCI, 10 rue Vauquelin, 75005 Paris, France*

^(b) *Laboratoire de Physique des Solides, UMR CNRS 8502, Bât. 510, Université Paris-Sud, 91405 Orsay, France and*

^(c) *Laboratoire Kastler Brossel, ENS, Université Paris 6, CNRS, 24 rue Lhomond, 75005 Paris, France*

(Dated: October 31, 2018)

We investigate theoretically and experimentally the capillary-gravity waves created by a small object moving steadily at the water-air interface along a circular trajectory. It is well established that, for straight uniform motion, no steady waves appear at velocities below the minimum phase velocity $c_{\min} = 23 \text{ cm} \cdot \text{s}^{-1}$. We show theoretically that no such velocity threshold exists for a steady circular motion, for which, even for small velocities, a finite wave drag is experienced by the object. This wave drag originates from the emission of a spiral-like wave pattern. Our results are in good agreement with direct experimental observations of the wave pattern created by a circularly moving needle in contact with water. Our study leads to new insights into the problem of animal locomotion at the water-air interface.

PACS numbers: 47.35.-i , 68.03.-g

Capillary-gravity waves propagating at the free surface of a liquid are driven by a balance between the liquid inertia and its tendency, under the action of gravity and surface tension forces, to return to a state of stable equilibrium [1]. For an inviscid liquid of infinite depth, the dispersion relation relating the angular frequency ω to the wave number k is given by $\omega^2 = gk + \gamma k^3/\rho$, where ρ is the liquid density, γ the liquid-air surface tension, and g the acceleration due to gravity [2]. The above equation may also be written as a dependence of the wave velocity $c(k) = \omega(k)/k$ on wave number: $c(k) = (g/k + \gamma k/\rho)^{1/2}$. The dispersive nature of capillary-gravity waves is responsible for the complicated wave pattern generated at the free surface of a still liquid by a moving disturbance such as a partially immersed object (*e.g.* a boat or an insect) or an external surface pressure source [2, 3, 4, 5, 6]. Since the disturbance expends a power to generate these waves, it will experience a drag, R_w , called the *wave resistance* [3]. In the case of boats and large ships, this drag is known to be a major source of resistance and important efforts have been devoted to the design of hulls minimizing it [7]. The case of objects small relative to the capillary length $\kappa^{-1} = (\gamma/(\rho g))^{1/2}$ has only recently been considered [8, 9, 10, 11].

In the case of a disturbance moving at *constant* velocity \mathbf{V} , the wave resistance R_w cancels out for $V < c_{\min}$ where V stands for the magnitude of the velocity, and $c_{\min} = (4g\gamma/\rho)^{1/4}$ is the minimum of the wave velocity $c(k)$ given above for capillarity gravity waves [3, 4, 8]. For water with $\gamma = 73 \text{ mN} \cdot \text{m}^{-1}$ and $\rho = 10^3 \text{ kg} \cdot \text{m}^{-3}$, one has $c_{\min} = 0.23 \text{ m} \cdot \text{s}^{-1}$ (room temperature). This striking behavior of R_w around c_{\min} is similar to the well-known Cerenkov radiation emitted by a charged particle [12], and has been recently studied experimentally [13, 14]. In this letter, we demonstrate that just like *accelerated* charged particles radiate electromagnetic waves even while moving slower than the speed of light [15], an accelerated disturbance experiences a non-zero wave

resistance R_w even when propagating below c_{\min} . We consider the special case of a uniform circular trajectory, a situation of particular importance for the study of whirligig beetles (*Gyrinidae*, [16]) whose characteristic circular motion might facilitate the emission of surface waves that they are thought to be used for echolocation [17, 18]. This work is therefore restricted to the effect of a wake stationary in the rotating frame, and do not consider time dependent contributions, like vortex shedding [27, 29].

We consider the case of an incompressible infinitely deep liquid whose free surface is unlimited. In the absence of external perturbation, the free surface is flat and each of its points can be described by a radius vector $\mathbf{r} = (x, y)$ in the horizontal plane. The motion of a small object along the free surface disturbs the equilibrium position of the fluid, and each point of the free surface acquires a finite vertical displacement $\zeta(\mathbf{r})$. Rather than solving the complex hydrodynamic problem of finding the flow around a moving object, we consider the displacement of an external pressure source $P_{ext}(\mathbf{r}, t)$ [5, 6]. The equations of motion can then be linearized in the limit of small wave amplitudes [19].

In the frame of this linear-response theory, it is convenient to introduce the Fourier transforms of the pressure source $\hat{P}_{ext}(\mathbf{k}, t)$ and of the vertical displacement $\hat{\zeta}(\mathbf{k}, t)$ [20]. It can be shown that, in the limit of small kinematic viscosity ν , the relation between $\hat{\zeta}(\mathbf{k}, t)$ and $\hat{P}_{ext}(\mathbf{k}, t)$ is given by [9]

$$\frac{\partial^2 \hat{\zeta}}{\partial t^2} + 4\nu k^2 \frac{\partial \hat{\zeta}}{\partial t} + \omega^2(k) \hat{\zeta} = -\frac{k \hat{P}_{ext}(\mathbf{k}, t)}{\rho} \quad (1)$$

In this letter we assume that the pressure source has radial symmetry and that the trajectory $\mathbf{r}_0(t)$ of the object is circular, namely : $\mathbf{r}_0(t) = \mathcal{R}(\cos(\Omega t), \sin(\Omega t))$. Here \mathcal{R} is the circle radius, and Ω is the angular frequency. The linear velocity of the object is then given by

$V = \mathcal{R}\Omega$. With these assumptions, the external pressure field is $P_{ext}(\mathbf{r}, t) = P_{ext}(|\mathbf{r} - \mathbf{r}_0(t)|)$, yielding in Fourier space $\hat{P}_{ext}(\mathbf{k}, t) = \hat{P}_{ext}(k)e^{-i\mathbf{k}\cdot\mathbf{r}_0(t)}$. Since the right hand side of Eq. (1) is periodic with frequency Ω , it is possible to find its steady state solution by expanding the right hand side into Fourier series. The problem then becomes equivalent to the response of a damped oscillator to a sum of periodic forces with frequencies $n\Omega$, where n is an integer. The vertical deformation at any time t can then be reconstructed by evaluating the inverse Fourier transform. For the particular case of uniform circular motion, the time dependence is rather simple. Indeed, in steady state, the deformation profile rotates with the same frequency Ω as the disturbance. Therefore, in the rotating frame, ζ depends on the position \mathbf{r} only. The analytical expression of $\zeta(\mathbf{r})$ in cylindrical coordinates $(x, y) = r(\cos \phi, \sin \phi)$ is given by

$$\zeta(r, \phi) = \sum_{n=-\infty}^{\infty} e^{in\phi} \int \frac{k^2 dk}{2\pi\rho} \frac{\hat{P}_{ext}(k)J_n(kr)J_n(k\mathcal{R})}{n^2\Omega^2 - \omega^2(k) + 4in\nu k^2\Omega} \quad (2)$$

where J_n is n -th order Bessel function of the first kind. The summation index n is directly related to the n -th Fourier harmonic of the periodic function $e^{-i\mathbf{k}\cdot\mathbf{r}_0(t)}$ and, since the problem is linear, the contributions of all the harmonics add together.

The knowledge of the exact structure of the wave pattern is precious, but a quantitative measurement of the wave resistance is needed in order to understand, for example, the forces developed by small animals moving at the surface of water. In the case of the circular motion under study, the wave resistance R_w can be calculated from its average power $P_w = -\int d^2r \left\langle P_{ext}(\mathbf{r}, t) \frac{\partial \zeta(\mathbf{r}, t)}{\partial t} \right\rangle$ by $R_w = P_w/V$. Using the Fourier expansion of ζ , one then obtains in the limit $\nu\kappa/c_{\min} \rightarrow 0$ (for water, $\nu\kappa/c_{\min} \sim 10^{-3}$):

$$R_w(V, \mathcal{R}) = \sum_{n>0} \frac{n}{\rho\mathcal{R}} \frac{(k_n J_n(k_n \mathcal{R}) \hat{P}_{ext}(k_n))^2}{\left(\frac{d\omega^2}{dk}\right)_{k_n}} \quad (3)$$

where k_n is the unique solution of the equation $\omega(k_n) = n\Omega$ (the notation $R_w(V, \mathcal{R})$ stresses the dependence of R_w on the velocity magnitude and on the trajectory radius). Equation (3) shows that the wave resistance R_w takes the form of a sum $R_w = \sum_{n>0} A_n$, where the A_n are positive numbers that measure the contribution of each Fourier mode of the external pressure source (with frequency $n\Omega$) to the wave resistance.

A numerical calculation of the wave resistance is presented in Fig. 1 for a pressure source $\hat{P}_{ext}(k) = p_0 \exp(-kb)$, where p_0 is the total force exerted on the surface and b is the typical object size [22]. As observed, Eq. 3 differs significantly from the original prediction on the wave drag in the case of a straight uniform motion with velocity V [8, 11] given by

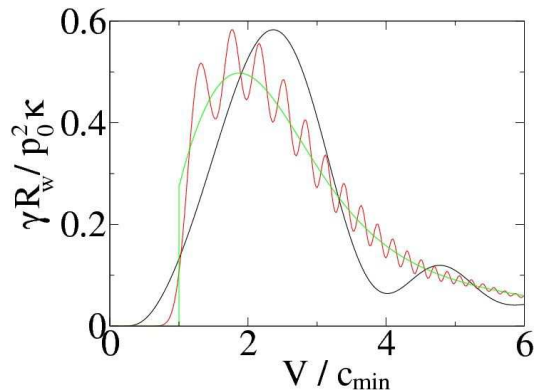


FIG. 1: (Color online) Plot of the wave resistance R_w in units of $p_0^2\kappa/\gamma$, as a function the reduced velocity $V/c_{\min} = \mathcal{R}\Omega/c_{\min}$ for different ratios between the trajectory radius \mathcal{R} , and the object size b , as predicted by Eq. (3). The red curve (presenting many oscillations) corresponds to $\mathcal{R}/b = 100$, while the black one (with fewer oscillations) corresponds to $\mathcal{R}/b = 10$. The green curve displaying a typical discontinuity at $V = c_{\min}$ is the wave drag for a straight uniform motion with velocity V [8]. The object size, b , was set to $b = 0.1 \kappa^{-1}$.

$$R_{w,l}(V) = \int_0^\infty \frac{kdk}{2\pi\rho} \frac{\hat{P}_{ext}^2(k) \theta(V - c(k))}{V^2 \sqrt{1 - (c(k)/V)^2}}, \quad (4)$$

where $\theta(\cdot)$ is the Heavyside function and $c(k) = \omega(k)/k$ is the phase velocity. Most notably, the wave drag for a circular motion is non-zero for all velocities, even for $V < c_{\min}$ where wave-resistance vanishes exactly in the case of a linear motion and this effect is far from negligible: for $\mathcal{R}/b = 10$ and at velocities as slow as $V/c_{\min} \sim 0.6$, the wave drag is still one fifth of that applied to an object moving linearly at $V/c_{\min} = 1$. The radiation of waves by an accelerated particle should not be surprising and actually is a very general phenomenon that can be observed for instance in electromagnetism (*bremstrahlung*) or in general relativity (Zeldovich-Starobinsky effect [23]). Mathematically, the fact that, for a circular motion, the wave resistance is finite even below c_{\min} can be understood as follows. In the case of uniform motion, all the wavenumbers such as $c(k) < V$ contribute to the wave drag, whereas for circular motion this is the case for only a discrete set of wavenumbers k_n . While the condition $c(k) < V$ can be satisfied only when $V > c_{\min}$, the equations for the wavenumber k_n , $\omega(k_n) = nV/\mathcal{R}$, have positive solutions for any velocity V . These wavenumbers k_n create finite contributions $A_n > 0$ to the wave drag. Therefore for a circular trajectory a finite wave drag exists at any velocity $V > 0$; for the same reasons R_w is also continuous at $V = c_{\min}$. Moreover, the wave resistance develops a small oscillating component as a function of the velocity V . It originates from the oscillatory behavior of Bessel functions and will be analyzed more thoroughly in a future

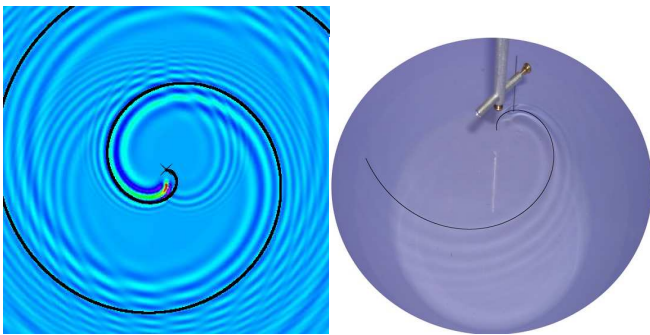


FIG. 2: (color online) Wave radiation for $V \approx 21\text{cm/s} \approx 0.9c_{\min}$ with a radius $\mathcal{R} \approx 2.7\text{cm} \approx 9\kappa^{-1}$. Left: Color diagram of the surface deformation $\zeta(\mathbf{r})$ computed numerically from Eq. (2). This image represents a square region of size $400\kappa^{-1}$ around the center of rotation, red color corresponds to maximal $\zeta(\mathbf{r})$ values, while green corresponds to minimal values of $\zeta(\mathbf{r})$. The cross indicates the center of the trajectory and the moving object is located in the region of highest deformation. Right: Photography of the wave crests generated on a water surface by a needle rotating at a velocity V . On both pictures, the black curve represents the Archimedean spiral of radius given by Eq. (5).

publication. Finally, we note that despite these striking differences Eqn. (3) and (4) should coincide in the limit of a large trajectory radius \mathcal{R} . We confirmed this behavior by checking both analytically [24] and numerically that in the limit $\mathcal{R} \rightarrow \infty$, $R_w(V, \mathcal{R}) \rightarrow R_{w,l}(V)$. However even if the circular wave drag $R_w(V, \mathcal{R})$ is close to $R_{w,l}(V)$ starting from $\mathcal{R}/b \sim 10$, important differences remain even up to very large values of \mathcal{R}/b such as $\mathcal{R}/b \sim 100$.

Figure 2 represents the wave crest pattern (computed numerically from Eq.(2)) at the origin of this finite wave drag. It exhibits characteristic concentric Archimedean spirals (also known as arithmetic spirals) of the form $r = a\phi + r_0$. This can be understood from our theoretical results as follows. In a first estimation, one can assume that the integrals in equation Eq. (2) are dominated by the contribution of the poles at $k = k_n$. Thus $\zeta(\mathbf{r})$ can be written as $\zeta(\mathbf{r}) \sim \frac{1}{\sqrt{r}} \sum_n B_n e^{i(n\phi - k_n r)}$, where we have used the asymptotic development of $J_n(k_n r)$ at large distances r and B_n are complex coefficients that do not depend on the position $\mathbf{r} = r(\cos \phi, \sin \phi)$. By separating the contribution of the different modes in the relation $\mathbf{F}(t) = -\int d^2r P_{ext}(\mathbf{r}, t) \nabla \zeta(\mathbf{r}, t)$, one finds that B_n is proportional to A_n (where, as defined earlier, the positive coefficients A_n measure the contribution of each Fourier mode to the wave drag: $R_w = \sum_{n>0} A_n$). One can show that in the regime of small object sizes $\kappa b \ll 1$, the proportionality constant between B_n and A_n depends only weakly on the Fourier mode number n ; thus, one has $\zeta(\mathbf{r}) \propto \frac{1}{\sqrt{r}} \sum_n A_n e^{i(n\phi - k_n r)}$. We have checked numerically that in the regime $V < c_{\min}$, the distribution of the coefficients A_n is usually peaked around $n \sim \kappa \mathcal{R}$. For ex-

ample, for $\kappa \mathcal{R} = 10$ and $\kappa b = 0.1$, A_n is peaked around $n = 10$ for velocities V in the interval $(c_{\min}/2, c_{\min})$. The wave-crests are given by the lines of constant phase $n\phi - k_n r = \text{const}$ of the dominant mode $n = \kappa \mathcal{R}$, leading to the following expression for a :

$$a \approx \frac{\kappa \mathcal{R}}{k(\omega = \kappa V)} \quad (5)$$

where $k(\omega)$ is the inverse function of $\omega(k)$. An interesting special case of the formula Eq. (5) corresponds to $V = c_{\min}$, for which one obtains $a \approx \mathcal{R}$. The spiral predicted by Eq. (5) is in very good agreement with the exact numerical results (Eq. (2)), as can be seen in Fig. 2.

We have also compared our theoretical approach with experimental results obtained using a one millimeter wide stainless steel needle immersed in a 38 cm wide water bucket. The needle was rotated on circular trajectories of various radii and angular velocities. Since direct measurement of wave drag, and in particular comparison with theory, is non-trivial even for a linear motion [13, 14], we restricted ourselves to the study of the wake itself. A typical wave pattern obtained by this method is shown on Fig. 3 for $\mathcal{R} \approx 2.7\text{cm}$ and $\Omega \approx 2\pi \times 1.2\text{Hz}$ (corresponding to $V/c_{\min} \approx 0.9$) and unambiguously demonstrates the existence of a wake at velocities smaller than c_{\min} . The observed wave pattern is in remarkable agreement with the theoretical prediction $r = a\phi + b$ with a given by Eq. (5) and r_0 a free parameter corresponding to an overall rotation of the spiral [25]. For V/c_{\min} lower than 0.8, no wake was observed by naked eye. At lower rotation velocities, we probed the surface deformation by measuring the deflexion of a laser beam reflected by the air-water interface at a distance $r = 11\text{cm}$ from the rotation axis.

Using this scheme, we have established the existence of waves down to $V/c_{\min} \approx 0.6$, and verified quantitatively that the wave packet spectrum is peaked around $\langle \omega \rangle \sim \kappa \mathcal{R} \Omega$ (see Fig. 3). Experimentally, the frequency $\langle \omega \rangle$ corresponds to the period of the fast temporal oscillations of the laser deflection angle (see Fig. 3 inset). In order to compare our experimental results with our model, we note that the deflection of the laser at a point \mathbf{r} is proportional to the derivatives $\frac{1}{r} \frac{\partial \zeta(\mathbf{r}, t)}{\partial \phi}$ and $\frac{\partial \zeta(\mathbf{r}, t)}{\partial r}$. For simplicity, we will mainly consider the angular derivative, but we have checked numerically that our result do not depend on this choice. Using Eq. (2) the angular derivative can be decomposed into Fourier series: $\frac{\partial \zeta(\mathbf{r}, t)}{\partial \phi} = \sum_n C_n e^{in(\phi - \Omega t) - ik_n r}$. The coefficients C_n are proportional to the contribution of the frequency $n\Omega$ to the wave packet spectrum and we can thus calculate the mean wave packet frequency using the expression: $\langle \omega \rangle = \Omega \frac{\sum_{n>0} n |C_n|}{\sum_{n>0} |C_n|}$. As shown in Fig. 3, our model is consistent with good accuracy with the experimental data without any adjustable parameters.

Below $V/c_{\min} \approx 0.6$, the signal to noise ratio of the experiment becomes so small to observe the laser deflection. Note that this value is in qualitative agreement

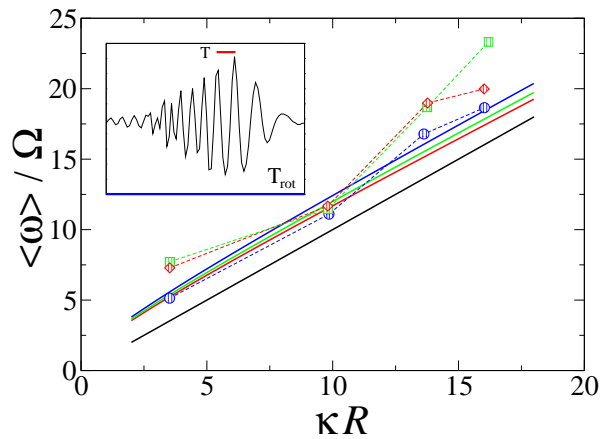


FIG. 3: (Color online) Inset: typical time dependence of the laser deflection angle (arbitrary units) during a rotation period $T_{\text{rot}} = 2\pi/\Omega$, the fast oscillation frequency is given by $\langle \omega \rangle = 2\pi/T$. Main figure: Dependence of the ratio $\langle \omega \rangle / \Omega$ on κR for different needle velocities. The dashed curves represent experimental results, while the continuous curves display the numerical results of our model. Red, green and blue curves (diamonds, squares and circles respectively) correspond to $V/c_{\min} = 0.69, 0.76$ and 0.84 . The black curve correspond to the analytical estimate $\langle \omega \rangle / \Omega = \kappa R$.

with Fig. 1 where the wave resistance (hence the wave amplitude) has also significantly decreased with respect to its maximum value for $V/c_{\min} \lesssim 0.5$: we indeed note that for

To summarize, we have shown theoretically that a disturbance moving along a circular trajectory experienced a wave drag even at angular velocities corresponding to $V < c_{\min}$, where c_{\min} is the minimum phase velocity of capillary-gravity waves. Our prediction is supported by experimental observation of a long distance wake for V/c_{\min} as low as 0.6. For $V/c_{\min} > 0.8$, we observed by naked eye Archimedean spiral shaped crests, in good agreement with theory. These results are directly related to the accelerated nature of the circular motion, and thus do not contradict the commonly accepted threshold $V = c_{\min}$ that is only valid for a rectilinear uniform motion, an assumption often overlooked in the literature. It would be very interesting to know if whirligig beetles can take advantage of such spirals for echolocation purposes. Although restricted to stationary wakes and thus excluded effects such as vortex shedding, the results presented in this letter should be important for a better understanding of the propulsion of water-walking insects [26, 27, 28, 29] where accelerated motions frequently occurs (*e.g* when hunting a prey or escaping a predator [30]). Even in the case where the insect motion is rectilinear and uniform, one has to keep in mind that the rapid leg strokes are accelerated and might produce a wave drag even below c_{\min} .

We are grateful to José Bico, Jérôme Casas, M. W. Denny and J. Keller for fruitful discussions. F.C. acknowledges support from Région Ile de France (IFRAF) and A.C. acknowledges support from Ecole Normale Supérieure Paris.

-
- [1] L. D. Landau and E. M. Lifshitz *Fluid Mechanics*, 2nd ed. (Pergamon Press, New York 1987).
- [2] D. J. Acheson, *Elementary Fluid Dynamics* (Clarendon Press, Oxford, 1990).
- [3] J. Lighthill, *Waves in Fluids*, 6th ed. (Cambridge University Press, Cambridge, 1979).
- [4] H. Lamb, *Hydrodynamics*, 6th ed. (Cambridge University Press, Cambridge, 1993).
- [5] Lord Rayleigh, Proc. London Math. Soc., **15**, 69 (1883).
- [6] Lord Kelvin, Proc. London Math. Soc. A, **15**, 80 (1887).
- [7] J. H. Milgram, Annu. Rev. Fluid Mech., **30**, 613 (1998).
- [8] E. Raphaël and P.-G. de Gennes, Phys. Rev. E, **53**, 3448 (1996).
- [9] D. Richard and E. Raphaël, Europhys. Lett. **48**, 53 (1999).
- [10] S.-M. Sun and J. Keller, Phys. Fluids, **13**, 2146 (2001).
- [11] F. Chevy and E. Raphaël, Europhys. Lett., **61**, 796 (2003).
- [12] P. A. Cherenkov, C. R. Acad. Sci. URSS **8**, 451 (1934).
- [13] J. Browaeys, J.-C. Bacri, R. Perzynski and M. Shliomis, Europhys. Lett. **53**, 209 (2001).
- [14] T. Burghlea and V. Steinberg, Phys. Rev. Lett. **86**, 2557 (2001) and Phys. Rev. E **66**, 051204 (2002).
- [15] J. D. Jackson, *Classical Electrodynamics*, 3rd ed. (Wiley, 1998).
- [16] W. Nachtigall, in *The Physiology of Insecta* (Academic Press, New York, 1965)
- [17] V. A. Tucker, Science **166**, 897 (1969).
- [18] M. W. Denny, *Air and Water*, (Princeton University Press, Princeton 1993).
- [19] For nonlinear effects, see F. Dias and C. Kharif, Annu. Rev. Fluid Mech., **31**, 301 (1999).
- [20] The Fourier transform $\hat{f}(\mathbf{k}, t)$ is related with the function $f(\mathbf{r}, t)$ through $f(\mathbf{r}, t) = \int \frac{d^2k}{(2\pi)^2} e^{i\mathbf{k}\cdot\mathbf{r}} \hat{f}(\mathbf{k}, t)$
- [21] T. H. Havelock, Proc. R. Soc. A, **95**, 354 (1918).
- [22] While all the data shown in this letter are obtained with this expression for $P_{ext}(r)$, we have verified that other distributions (gaussian, step function, ...) lead qualitatively to the same results.
- [23] Ya. B. Zeldovich, JETP Lett. **14**, 180 (1971); A. A. Starobinsky, JETP **37**, 28 (1973).
- [24] J. Keller, private communication.
- [25] Note that we also observed on some pictures the weaker spiral seen in Fig. 2 and propagating in the opposite direction with respect to the main wake. However, this “advanced” wake could only be observed at high velocities ($V/c_{\min} \sim 2$) because of its small relative amplitude.
- [26] R. McNeill Alexander, *Principle of Animal Locomotion*, (Princeton University Press, Princeton 2002).
- [27] J. W. Bush and D. L. Hu, Annu. Rev. Fluid Mech., **38**, 339 (2006).

[28] M. W. Denny, *J. Exp. Biol.*, **207** 1601 (2004).
[29] O. Buhler, *J. Fluid Mech.*, **573**, 211 (2007).

[30] H. Bendele, *J. Comp. Physiol. A*, **158**, 405 (1986).